



HAL
open science

Effect of a high magnetic field on the growth of ϵ -CuZn₅ dendrite during directionally solidified Zn-rich Zn–Cu alloys

Dafan Du, Guang Guan, Annie Gagnoud, Yves Fautrelle, Zhongming Ren, Xionggang Lu, Hui Wang, Yinming Dai, Qiuliang Wang, Xi Li

► To cite this version:

Dafan Du, Guang Guan, Annie Gagnoud, Yves Fautrelle, Zhongming Ren, et al.. Effect of a high magnetic field on the growth of ϵ -CuZn₅ dendrite during directionally solidified Zn-rich Zn–Cu alloys. Materials Characterization, 2016, 111, pp.31-42. 10.1016/j.matchar.2015.11.004 . hal-01367833

HAL Id: hal-01367833

<https://hal.science/hal-01367833>

Submitted on 2 Mar 2023

HAL is a multi-disciplinary open access archive for the deposit and dissemination of scientific research documents, whether they are published or not. The documents may come from teaching and research institutions in France or abroad, or from public or private research centers.

L'archive ouverte pluridisciplinaire **HAL**, est destinée au dépôt et à la diffusion de documents scientifiques de niveau recherche, publiés ou non, émanant des établissements d'enseignement et de recherche français ou étrangers, des laboratoires publics ou privés.



Distributed under a Creative Commons Attribution - NonCommercial 4.0 International License

Effect of a high magnetic field on the growth of ϵ -CuZn₅ dendrite during directionally solidified Zn-rich Zn–Cu alloys

Dafan Du ^a, Guang Guan ^a, Annie Gagnoud ^b, Yves Fautrelle ^b, Zhongming Ren ^a, Xionggang Lu ^a, Hui Wang ^c, Yinming Dai ^c, Qjuliang Wang ^c, Xi Li ^{a,b,*}

^a State Key Laboratory Advanced Special Steel, Shanghai University, Shanghai 200072, PR China

^b SIMAP-EPM-Madylam/G-INP/CNRS, PHELMA, BP 75, 38402 St Martin d'Heres Cedex, France

^c Key Laboratory of Applied Superconductivity, Institute of Electrical Engineering, CAS, Beijing 100190, PR China

The effect of an axial high magnetic field on the growth of ϵ -CuZn₅ dendrite during directionally solidified Zn-rich Zn–Cu peritectic alloys was investigated. Experimental results revealed that the magnetic field caused the deformation of the ϵ -CuZn₅ dendrite and induced the occurrence of the columnar-to-equiaxed transition (CET) of the ϵ -CuZn₅ dendrite. Further, EBSD technology was applied to study the dendrite morphology and crystalline orientation in details. It was found that the regular ϵ -CuZn₅ columnar dendrite formed and was oriented with the $\langle 0001 \rangle$ -crystal direction along the solidification direction at moderate growth speeds (i.e., 10–50 $\mu\text{m/s}$). When a high magnetic field was applied, equiaxed grains with various random orientations formed. Further, the magnetic crystalline anisotropy of the ϵ -CuZn₅ crystal was studied. Experimental results showed that the ϵ -CuZn₅ crystal owns a magnetic crystalline anisotropy and the $\langle 0001 \rangle$ -crystal direction is its easy magnetization axis. Moreover, numerical results indicated that a thermoelectric magnetic force acted on the solid near the liquid/solid interface and increased linearly with the magnetic field. The degeneration and breakup of the ϵ -CuZn₅ dendrites during directional solidification of the Zn–Cu alloys under the magnetic field may be primarily due to the thermoelectric magnetic force acting on the solid.

1. Introduction

Zn–Cu is a typical binary peritectic system in which four peritectic reactions occur over the whole composition range. Peritectic reactions are commonly observed in systems that include components with large differences in melting points [1]. It not only features in the solidification of structural materials [2–5] but also in the production of superconductors such as YBCO [6,7] and magnetic materials such as Co–Sm–Cu and Nd–Fe–B [8,9]. The dendritic structure is common during directional solidification of peritectic alloys. Recently, due to the development of superconducting magnets, a high magnetic field is widely used to improve material properties during material processing [10]. The effect of a high magnetic field on the dendrite growth in single phase alloys has been studied, and the results indicated that the application of a high magnetic field significantly affected the dendrite array significantly [11]. However, a few works have been done to study the effect of a high magnetic field on the dendrite growth in peritectic alloys. In present work, the effect of a high magnetic field on the growth of the

ϵ -CuZn₅ phases in the Zn-rich Zn–Cu peritectic alloys has been investigated. Moreover, the Seebeck thermoelectric signal (E_S) at the liquid/solid interface in the Zn–5 wt.% Cu peritectic alloy was measured in situ and the results indicated that the value of the Seebeck thermoelectric force was on the order of 10 μV .

The experimental results indicated that the application of the magnetic field had modified the dendrite morphology in the Zn-rich Zn–Cu alloys and changed the crystalline orientation. The above experiment phenomena were analyzed from the magnetic crystalline anisotropy and thermoelectric magnetic effects. This work will probably yield basic and valuable information leading to an extension of magnetic field application to exert microstructure and property control on metallic materials.

2. Experimental

The Zn–Cu alloys used in this study were prepared with high purity Zn (99.999 wt.%) and Cu (99.999 wt.%) in an induction furnace. The alloy, being put in a high-purity graphite crucible of 10 cm diameter, was heated to 600 °C, magnetically stirred for 0.5 h and poured into a graphite mold to cast specimens with the diameter of 3 mm and length

* Corresponding author.

E-mail address: lx_net@sina.com (X. Li).

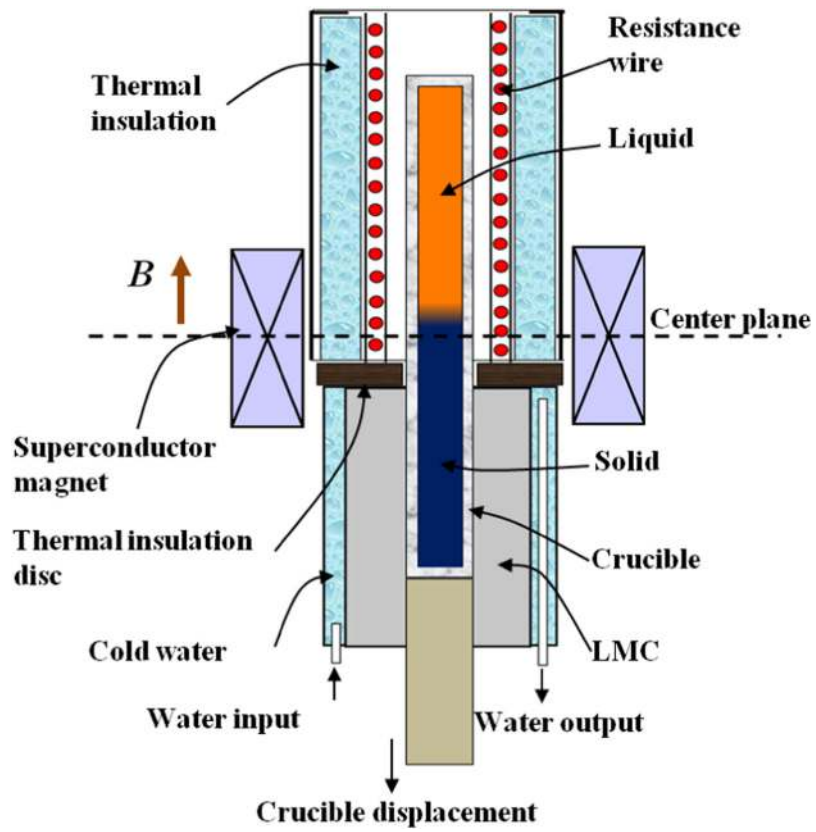


Fig. 1. Schematic illustration of the Bridgman solidification apparatus in a superconductor magnet.

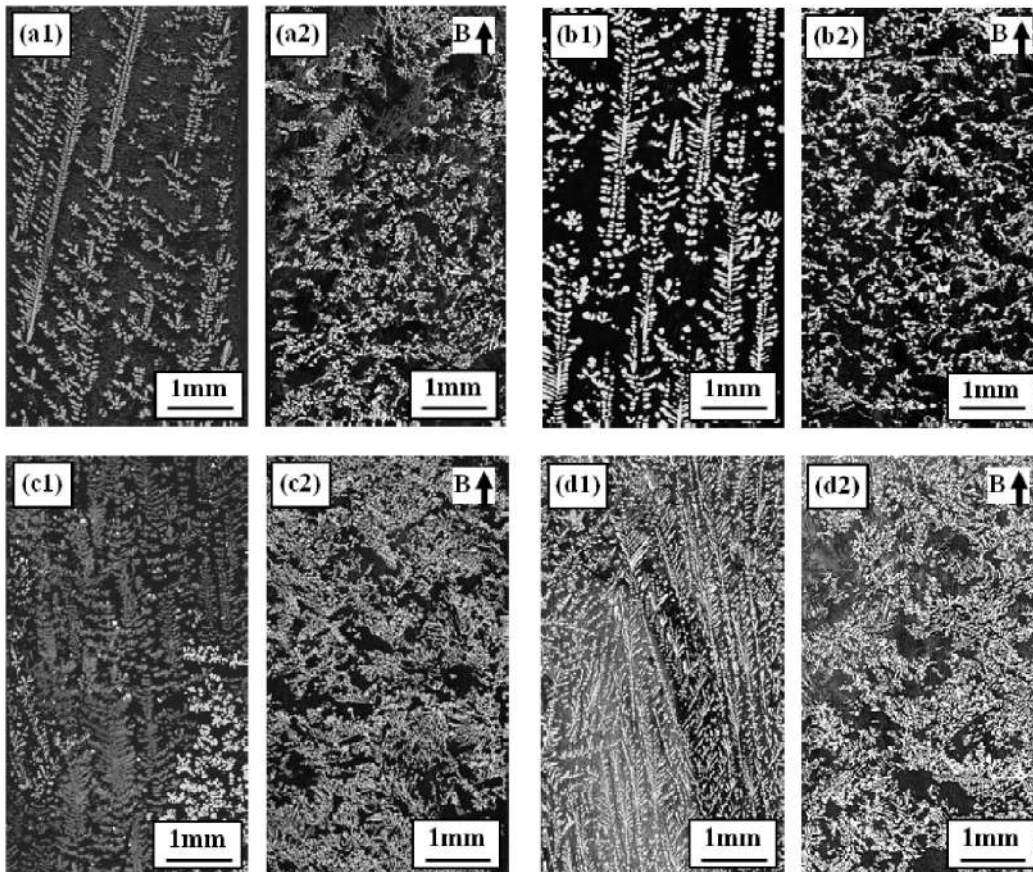


Fig. 2. Longitudinal microstructures in directionally solidified Zn-5 wt.% Cu alloy at various growth speeds without and with a 10 T magnetic field: (a) 5 $\mu\text{m/s}$; (b) 10 $\mu\text{m/s}$; (c) 50 $\mu\text{m/s}$; and (d) 100 $\mu\text{m/s}$.

of 200 mm. The cast specimen was enveloped in the tube of high purity corundum. The inner diameter of the sample is 3 mm and its length is 200 mm. The experimental apparatus, which is shown in Fig. 1, consists of a static superconductor magnet and a Bridgman-Stockbarger type furnace equipped with pulling system and temperature controllers. The superconductor magnet can produce an axial static magnetic field with an adjustable intensity up to 14 T. The furnace, which consists of non-magnetic material, has a negligible effect on the field uniformity. A water-cooled cylinder containing liquid Ga-In-Sn metal (LMC) was used to cool down the specimen. The temperature gradient in the specimen was controlled by adjusting the temperature of the furnace hot zone, which is insulated from the LMC by a refractory disc. The apparatus was designed such that the specimen moves downward while the furnace remains stationary. The growth speeds, R , lies in the range $0.5 \mu\text{m/s} \leq R \leq 15,000 \mu\text{m/s}$. To observe the morphology of the liquid/solid interface during the growth of the crystal, quenching experiments were performed by quickly withdrawing the specimen into the LMC cylinder to cool the specimen immediately to room temperature. During the experiment the specimens contained in the corundum crucibles

were melted and directionally solidified in the Bridgman apparatus by drawing the crucible assembly at various speeds into the LMC cylinder. In all of the experimental procedures, the magnetic field was present. The samples obtained from the experiments were extracted from both longitudinal and transversal sections of the directionally solidified casting. The samples were further ground with silicon carbide papers up to 2400 mesh, polished and etched with the Palmerton's reagent (40 g CrO_3 ; 1.5 g Na_2SO_4 and 200 ml of distilled and deionized water) to reveal the microstructure. Microstructural characterization of specimens was observed with a Leica DM 6000M optical microscope. Crystallographic characteristics were measured through the EBSD using a field-emission scanning electron microscope (SEM, SU-70, HITACHI) equipped with the EDAX's Hikira XP2 camera and OIM Analysis System (EBSD, EDAX Inc.). For EBSD analysis, the samples were first polished using a glycol based SiC suspension and then final vibration polishing using 50 nm colloidal silica on a vibratory polisher (Buehler, model: Vibromet 2) for 1.5 h. Standard clean-up procedures [12] was performed in OIM study to gain high-quality EBSD figures, as follows: (i) grain dilatation with a grain tolerance angle (GTA) of 2° ; a minimum

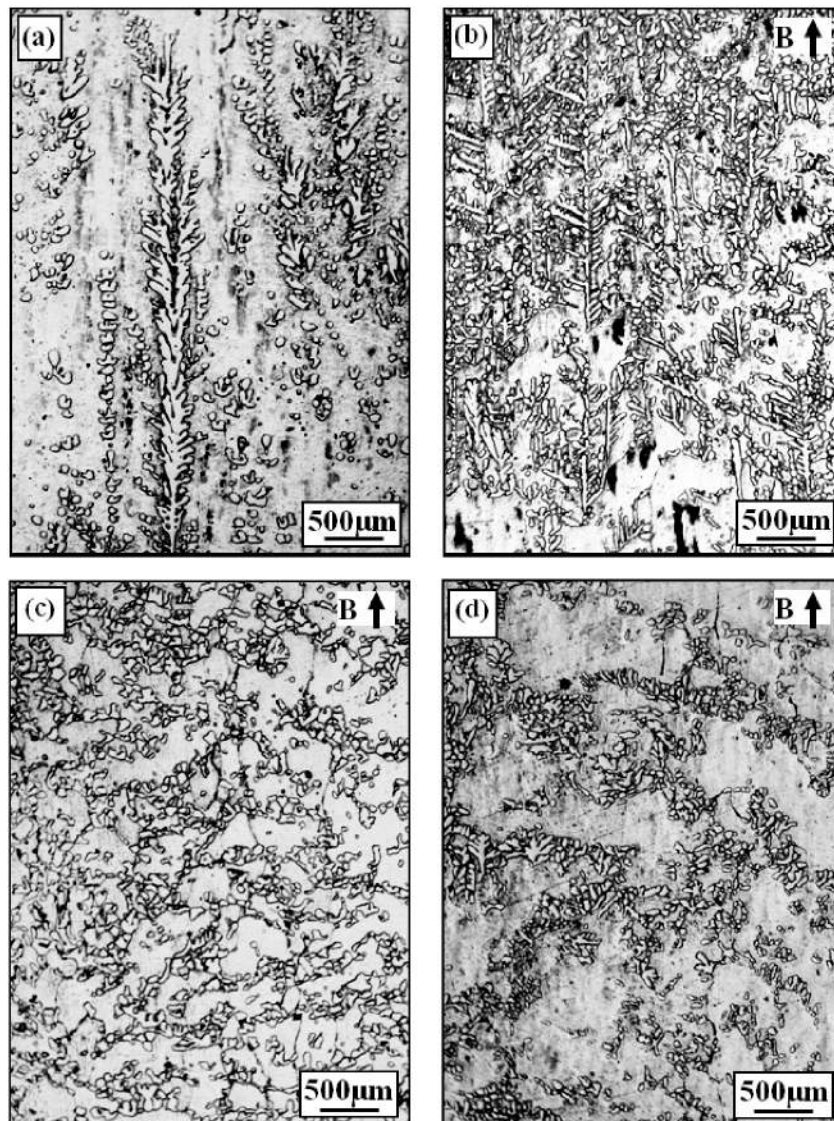


Fig. 3. Longitudinal structures in directionally solidified Zn-3.5 wt.% Cu alloy at a growth speed of $5 \mu\text{m/s}$ under various magnetic fields: (a) 0 T; (b) 1 T; (c) 5 T; and (d) 10 T.

grain size (MGS) of three pixels; (ii) neighbor CI correlation with minimum CI of 0.1.

3. Results

Fig. 2 shows the longitudinal structures for directionally solidified Zn-5 wt.% Cu alloy at various growth speeds without and with a 10 T magnetic field. It is obviously seen that solidified structures consist of primary ϵ -CuZn₅ phase (white) and η -Zn phase (dark) below the solid-liquid interface in each samples. It can be observed that the dendrite morphology without the magnetic field is typical columnar structure. However, when a 10 T high magnetic field was applied, regular columnar dendrites were destroyed significantly and tended to transform into equiaxed grains. Moreover, longitudinal microstructures of directionally solidified Zn-3.5 wt.% Cu alloy at a growth speed of 5 $\mu\text{m/s}$ under various magnetic fields have been investigated and the results are shown in Fig. 3. It can be learned that with the application of a 1 T magnetic field, the regular dendrites were broken and irregular dendrites formed. Continuing to increase the magnetic field to 5 T and 10 T,

the columnar-to-equiaxed transition (CET) occurred. Fig. 4 shows the longitudinal microstructures near the liquid/solid interface and transverse structure 5 mm below the interface in directionally solidified Zn-5.0 wt.% Cu alloy at a growth speed of 10 $\mu\text{m/s}$ without and with a 10 T magnetic field. It can be observed that with the absence of the magnetic field the ϵ -CuZn₅ dendrite exhibits a typical columnar dendrite microstructure as shown in Fig. 4a and c and the typical primary ϵ -CuZn₅ phase uniform distribute across the entire sample cross section. However, when a 10 T high magnetic field is imposed, the microstructures (Fig. 4b and d) are changed significantly; the ϵ -CuZn₅ columnar dendrite was destroyed seriously and transformed into irregular equiaxed grains.

Further, the EBSD technology was applied to study the dendrite morphology and the crystalline orientation. Fig. 5 shows the EBSD map for the structures in directionally solidified at low growth speeds (2 $\mu\text{m/s}$ and 10 $\mu\text{m/s}$) without and with a 10 T magnetic field. One can notice that the magnetic field caused the deformation of the columnar η -Zn and ϵ -CuZn₅ phases and the occurrence of the CET. As the growth and orientation behavior of the ϵ -CuZn₅ phases in the Zn-Cu alloy are

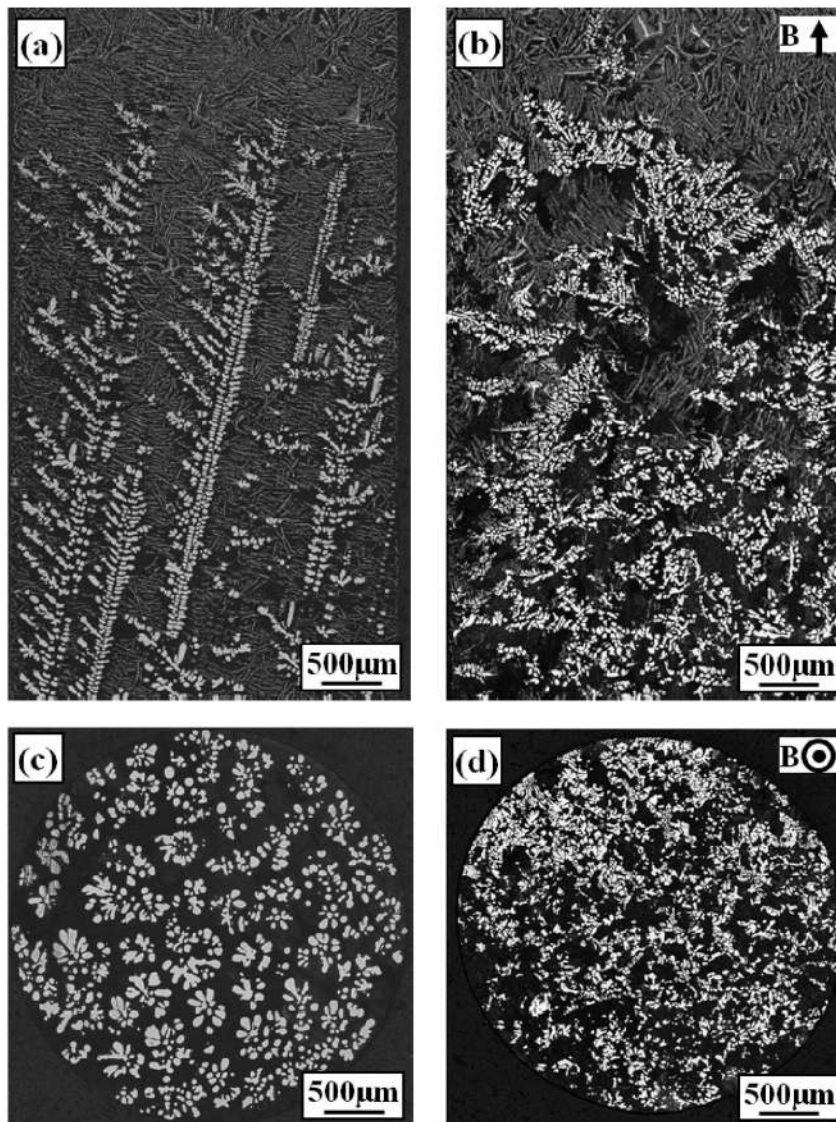


Fig. 4. Microstructures near the liquid/solid interface in directionally solidified Zn-5 wt.% Cu alloy at a growth speed of 10 $\mu\text{m/s}$ without and with a 10 T magnetic field: (a) longitudinal structure, 0 T; (b) longitudinal structure, 10 T; (c) transverse structure, 0 T; and (d) transverse structure, 10 T.

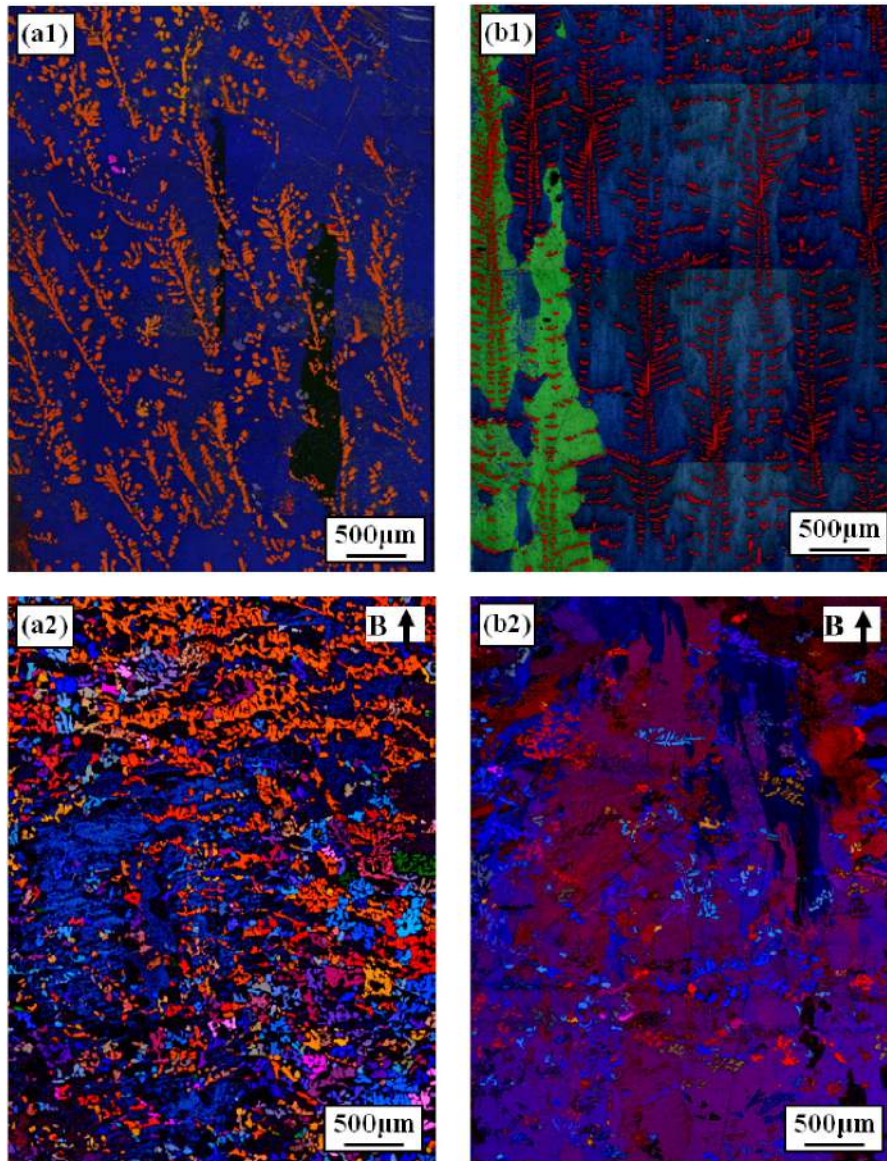


Fig. 5. EBSD map for the longitudinal structures in directionally solidified Zn-5 wt.% Cu alloys at a certain growth speed with and without a 10 T magnetic field: (a) 2 $\mu\text{m/s}$ and (b) 10 $\mu\text{m/s}$.

unclear so far, firstly the dendrite growth and orientation behavior of the $\epsilon\text{-CuZn}_5$ phases was studied by using the EBSD analysis. Fig. 6 and Fig. 7 show the EBSD map and the corresponding $\langle 0001 \rangle$ -pole figures for the structures in directionally solidified Zn-5 wt.% Cu alloy at various growth speeds with the absence of magnetic field, respectively. One can notice that the $\epsilon\text{-CuZn}_5$ phases exhibit irregular columnar structure at low growth speeds and the regular dendrites formed at a moderate growth speed. The pole figures in Fig. 7a-eshows that the $\epsilon\text{-CuZn}_5$ dendrite possessed a very strong fiber texture with $\langle 0001 \rangle$ -directions of the hexagonal $\epsilon\text{-CuZn}_5$ crystals oriented preferentially parallel to the growth direction and the results also show that $\langle 0001 \rangle$ -directions of the hexagonal $\epsilon\text{-CuZn}_5$ crystals oriented along the growth direction gradually with the increase of growth speed. However, when the growth speed increases to 100 $\mu\text{m/s}$, the $\langle 0001 \rangle$ fiber texture disappeared and the $\langle 0001 \rangle$ -direction deflect from the growth direction (i.e. magnetic field direction). Fig. 8 shows the EBSD map and the corresponding $\langle 0001 \rangle$ -pole figures of the $\epsilon\text{-CuZn}_5$ phase for the longitudinal structures in directionally solidified Zn-5 wt.% Cu alloy at various growth speeds under a 10 T magnetic field. It can be observed clearly

that the application of a high magnetic field caused the regular columnar dendrite to transform into equiaxed grains. At the same time, the $\langle 0001 \rangle$ -preferred growth direction of the $\epsilon\text{-CuZn}_5$ phases deflected from the solidification direction and became disperse. This implies that the columnar dendrites orienting with the $\langle 0001 \rangle$ -crystal direction along the solidification direction have been transformed into equiaxed grains with various random orientations under the magnetic field. Further, Fig. 9 shows the EBSD analysis of the transverse section for samples solidified without and with a 10 T magnetic field at various growth rates.

4. Discussion

Above experimental results revealed that the application of a high magnetic field during directional solidification caused the formation of dendrite fragments and the occurrence of the CET. Normally, two major magnetic effects will influence the dendrite growth during the directional solidification under the magnetic field. One effect is the magnetic moment arising from the magnetic crystalline anisotropy. This

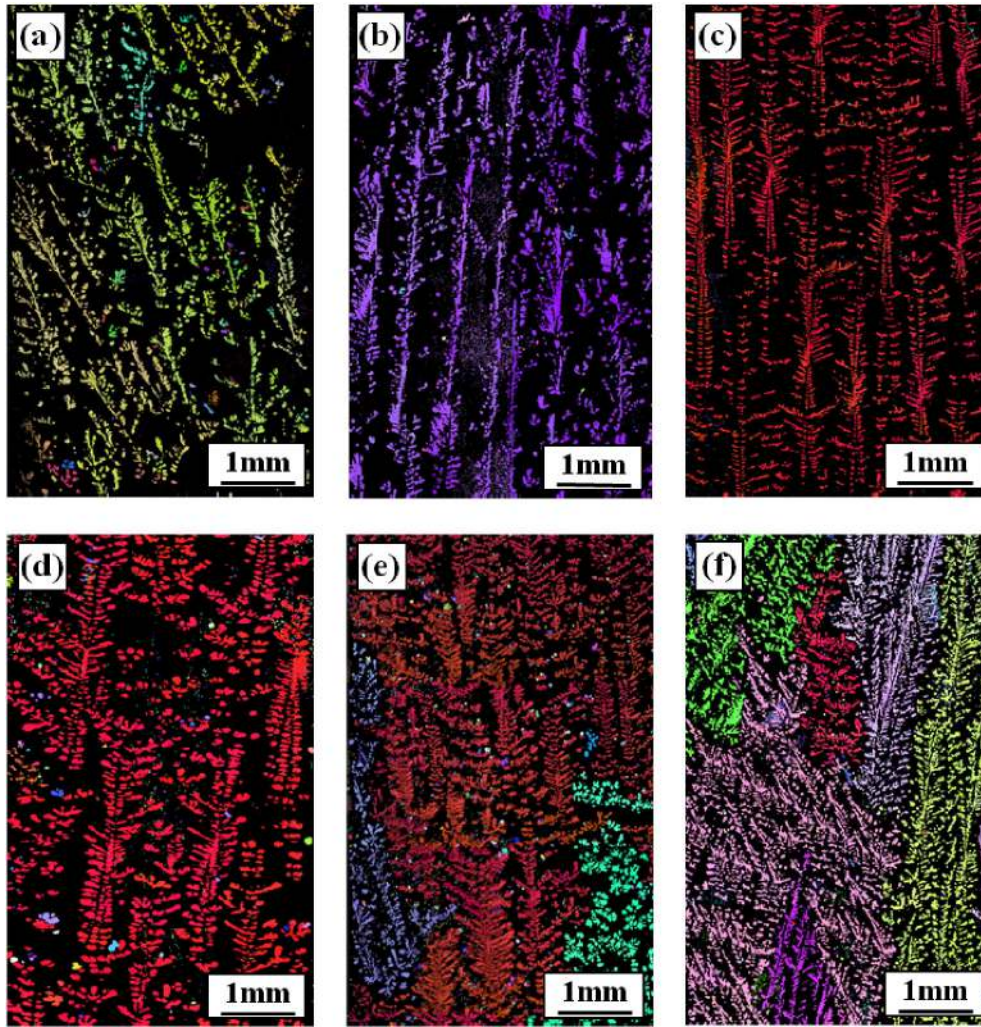


Fig. 6. EBSD map of the ϵ -CuZn₅ phase on the longitudinal structures in directionally solidified Zn-5 wt.% Cu alloy at various growth speeds: (a) 2 $\mu\text{m/s}$; (b) 5 $\mu\text{m/s}$; (c) 10 $\mu\text{m/s}$; (d) 20 $\mu\text{m/s}$; (e) 50 $\mu\text{m/s}$; and (f) 100 $\mu\text{m/s}$.

moment will tend to align the dendrites with the easy magnetic axis along the magnetic field [14]. Thus, the primary arm of the dendrite tends to deviate from the solidification direction as the easy magnetic axis rotates towards the magnetic field direction. As a consequence, the dendrite array is destroyed. Moreover, owing to the Seebeck effect [15], a thermoelectric current will be generated on the tip of the cell/dendrite [16]. When the magnetic field is applied, the interaction between the current and the magnetic field will induce a thermoelectric magnetic force. This thermoelectric magnetic force also destroys the dendrite array. Above two magnetic effects may work simultaneously and modify the dendrite array during directional solidification in the magnetic field.

Firstly, the magnetic crystalline anisotropy of the ϵ -CuZn₅ crystal is studied. To study the magnetic crystalline anisotropy of the ϵ -CuZn₅ crystal, the alignment behavior of the ϵ -CuZn₅ primary phase under a magnetic field was investigated. Fig. 10 shows the EBSD map and the corresponding $\langle 0001 \rangle$ pole figures for the microstructures during the diffusion process in the Zn/Cu diffusion couple with a 16 T magnetic field. The detail experimental process and setup for the diffusion experiment are available in Ref. [17]. It can be seen that the regular CuZn₅ hexagons appeared on the transverse section of the sample fabricated with the magnetic field and is oriented with the $\langle 0001 \rangle$ -crystal

direction along the magnetic field direction. Therefore, the $\langle 0001 \rangle$ -crystal of the CuZn₅ crystals is not only an easy magnetization axis but also a preferred growth direction. Thus, the magnetic moment becomes zero during the directional solidification under an axial magnetic field, and the effect of the magnetic moment on the dendrite array is eliminated. The modification of the microstructure during directional solidification under the magnetic field should be attributed to the thermoelectric magnetic effects.

Furthermore, to examine the distribution and amplitude of the thermoelectric magnetic effects near the liquid/solid interface during directional solidification of the Zn-rich Zn-Cu alloys under an axial magnetic field, numerical simulations were performed using the finite element commercial code FLUX-EXPERT™, which is available in our laboratory (SIMAP-EPM/G-INP/CNRS). The study configuration is 2 D, and the liquid and solid regions are both considered. The physical properties used in the computations are listed in Table 1 and thermoelectric power difference ($\eta_{sl} = S_S - S_L$) of the Zn-5 wt.% Cu alloy near the liquid/solid interface was measured in-situ by MEPHISTO apparatus for simulation. The basic principle of the interfacial thermoelectric measurement using the Seebeck technique was schematically presented in Fig. 11a. The details of the principle had been discussed in Refs. [19, 20]. Fig. 11b shows the Seebeck response obtained for the Zn-5 wt.%

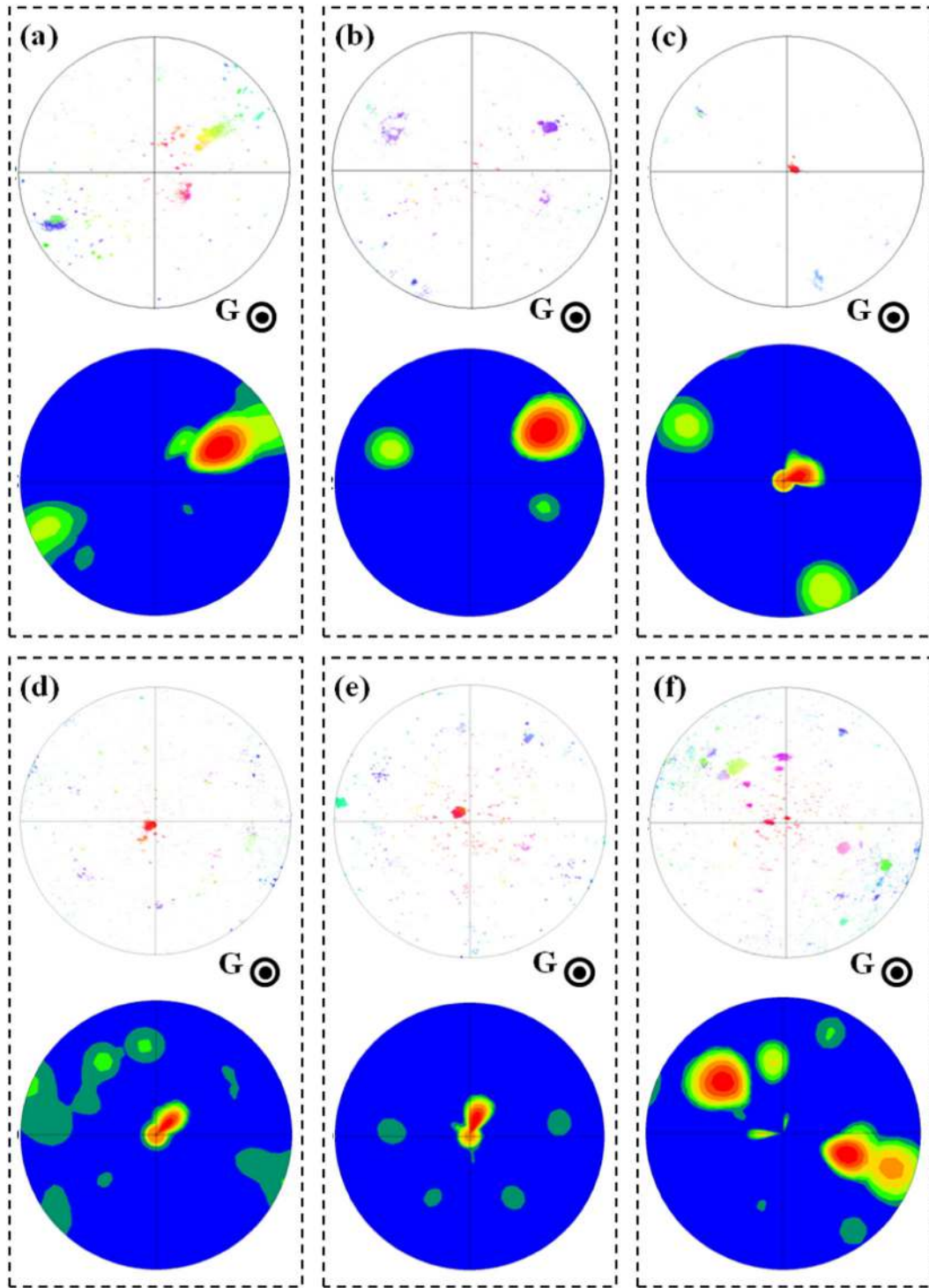


Fig. 7. The $\langle 0001 \rangle$ -pole figures of the ϵ -CuZn₅ phase corresponding to the EBSD map in Fig. 6: (a) 2 $\mu\text{m/s}$; (b) 5 $\mu\text{m/s}$; (c) 10 $\mu\text{m/s}$; (d) 20 $\mu\text{m/s}$; (e) 50 $\mu\text{m/s}$; and (f) 100 $\mu\text{m/s}$.

Cu alloy at a growth speed of 5 and 20 $\mu\text{m/s}$, respectively. One can learn that a plateau is obtained on the Seebeck curve to indicate establishment of steady state, and then the signal drops to a new steady state when furnace translation is shut off. The magnitude of signal drop, E_s , corresponds directly to the effective liquid/solid thermoelectric power difference (η_{sl}). This indicates that there indeed exists a liquid/solid thermoelectric power difference during directional solidification of the Zn-5 wt.% Cu alloy. The results show that there indeed exists a liquid/

solid thermoelectric power difference during directional solidification of the Zn-5 wt.% Cu alloy and the Seebeck signal at the given condition is on the order of 10 μV .

Fig. 12 shows the mesh used for the numerical simulation, the typical distribution of current density and thermoelectric magnetic force around a modeled liquid/solid interface under a 0.5 T magnetic field. The current swirl appears in the vicinity of the interface and that the rotation of the liquid around the dendrite, due to the radial component of

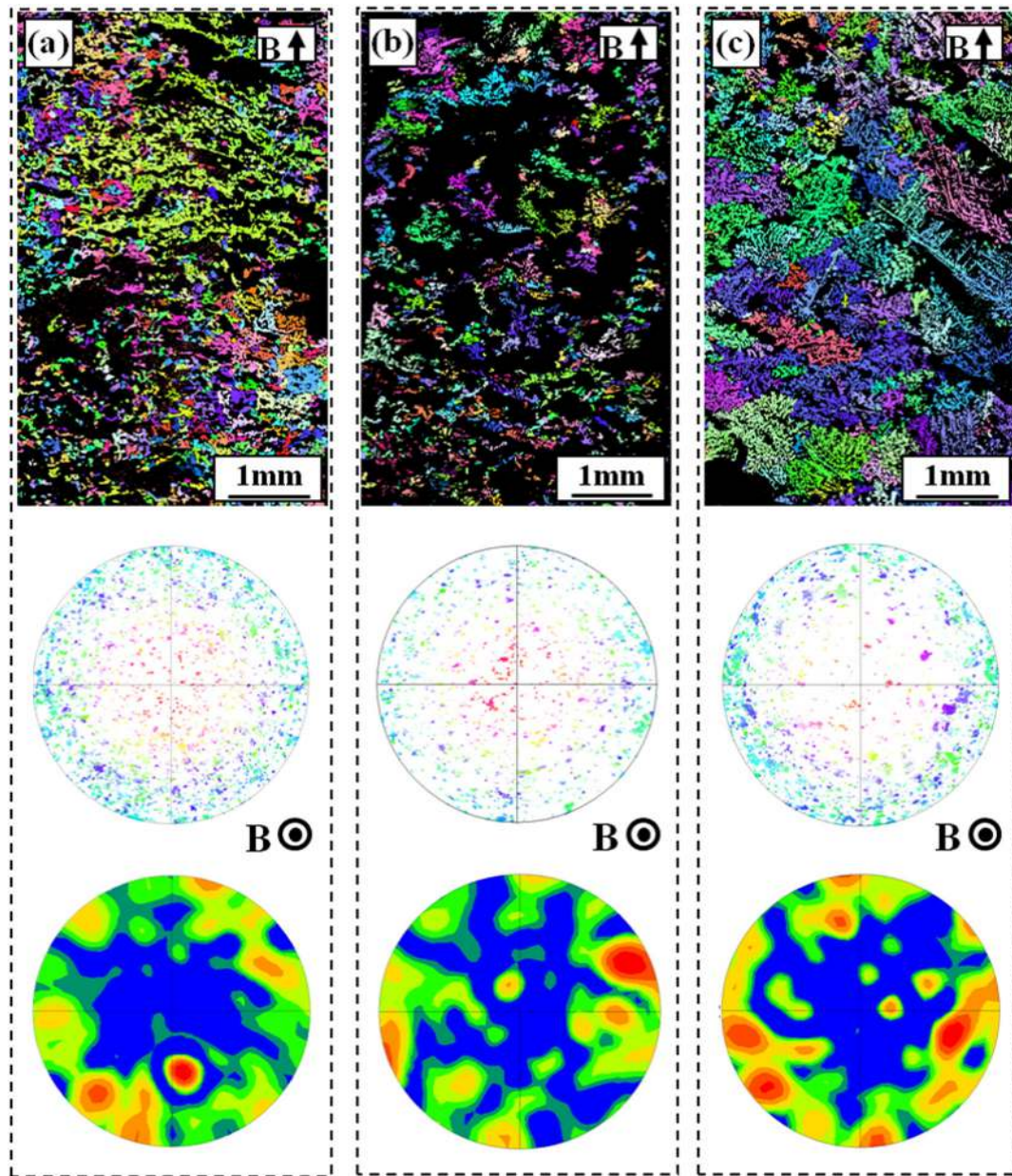


Fig. 8. EBSD map and the corresponding $\langle 0001 \rangle$ -pole figures of the ϵ -CuZn₅ phase for the longitudinal structures in directionally solidified Zn-5 wt.% Cu alloy at various growth speeds under a 10 T magnetic field: (a) 10 $\mu\text{m/s}$; (b) 20 $\mu\text{m/s}$; and (c) 100 $\mu\text{m/s}$.

the current density, will produce (see Fig. 12b). It should be noted that this swirl is remarkably localized in the vicinity of the interface and not extend into the bulk of the liquid. Thus, when a magnetic field is imposed, the interaction between the magnetic field and the thermoelectric current will produce a thermoelectric magnetic force as shown in Fig. 12c. The value of the force acting on the solid increases linearly as the magnetic field intensity increases (see Fig. 12d). Here, it is important to note that the thermoelectric magnetic force imposed on the solid during directional solidification with a temperature gradient of 60 K/cm under a 10 T magnetic field is of the order of 10^7 N/m^3 . The thermoelectric magnetic force acting on the solid may induce a torque that disrupts the dendrite resulting in the formation of dendrite fragments. As a consequence, the number of equiaxed grains ahead of the columnar front increases.

According to Hunt's mode, when the volume fraction of equiaxed grains exceeds 0.49, the CET will occur [18].

5. Conclusions

High magnetic fields were applied to study the growth of ϵ -CuZn₅ columnar dendrite for the peritectic Zn-Cu alloys. The results reveal that the high magnetic fields change the growth behavior of ϵ -CuZn₅ dendrite effectively.

1. The regular ϵ -CuZn₅ columnar dendrite formed and was oriented with the $\langle 0001 \rangle$ -crystal direction along the solidification direction at moderate growth speeds. The application of a high magnetic field caused the deformation of the ϵ -CuZn₅ phases and the occurrence of the CET of the ϵ -CuZn₅ phases.

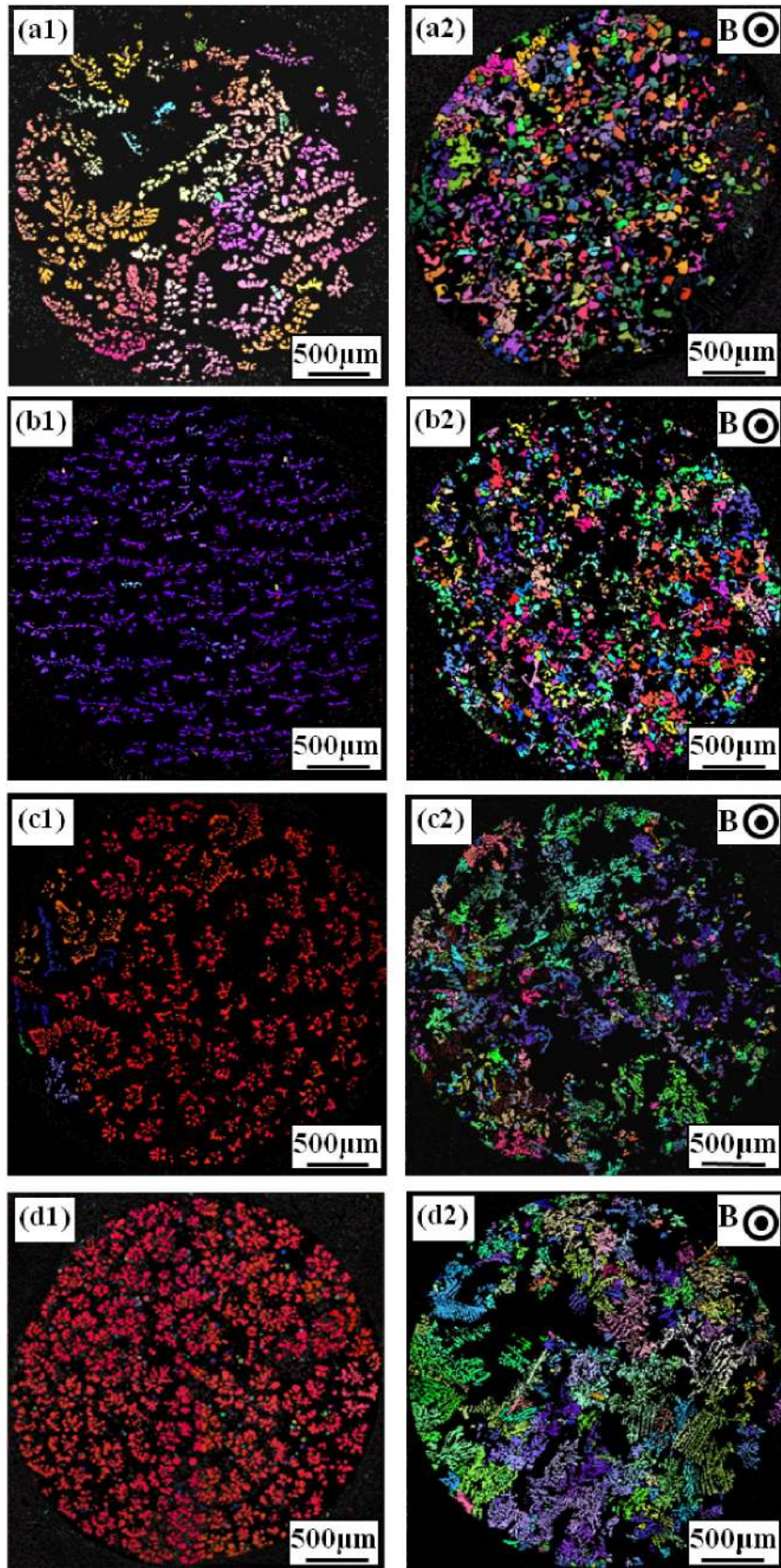


Fig. 9. Transverse EBSD map of the samples directionally solidified with various growth rates without and with a 10 T magnetic field, respectively: (a) 1 $\mu\text{m/s}$; (b) 5 $\mu\text{m/s}$; (c) 20 $\mu\text{m/s}$; and (d) 50 $\mu\text{m/s}$.

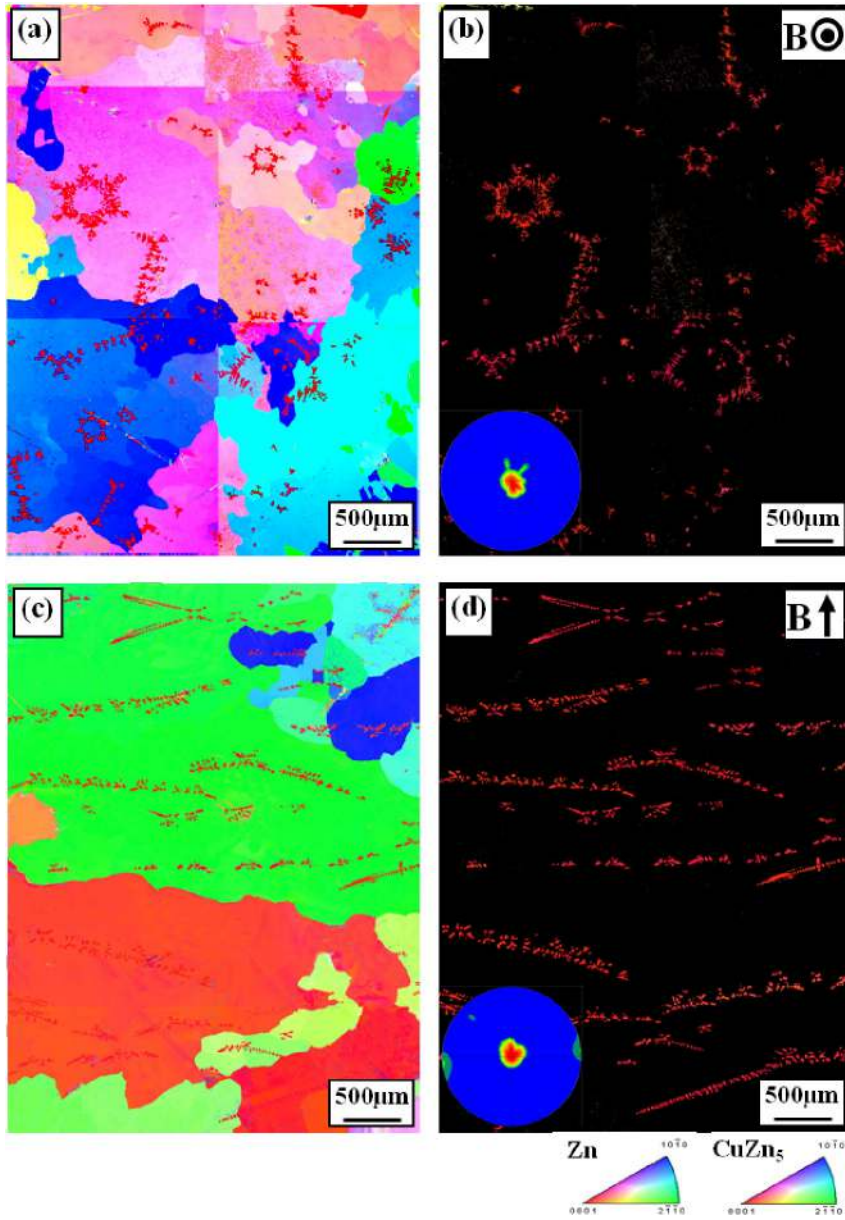


Fig. 10. EBSD map and the corresponding $\langle 0001 \rangle$ -pole figures for the structures annealed at 723 K for 7 h with a 16 T magnetic field: (a) EBSD map; (b) IPF map for ϵ -CuZn₅ phase in (a); (c) and (d) showing $\langle 0001 \rangle$ -pole figures of the Zn and CuZn₅ phases corresponding to (a), respectively.

2. The ϵ -CuZn₅ crystal owns a magnetic crystalline anisotropy and the $\langle 0001 \rangle$ -crystal direction is its easy magnetization axis. Indeed, it was found that the regular CuZn₅ hexagons appeared on the

transverse section of the sample fabricated with the magnetic field and was oriented with the $\langle 0001 \rangle$ -crystal direction along the magnetic field direction.

3. Numerical analysis revealed that a thermoelectric magnetic force acted on the solid and the value of this force increased linearly as the magnetic field intensity increased. The breakup and the CET of the ϵ -CuZn₅ phases during directional solidification under the magnetic field may be primarily attributed to the thermoelectric magnetic force acting on the solid.

Table 1
Physical properties of Zn-Cu alloys [21–23].

Properties	Magnitude
Electrical conductivity of solid Zn (σ_{S1} , $\Omega^{-1} \text{ m}^{-1}$)	16.6×10^6
Electrical conductivity of solid CuZn ₅ (σ_{S2} , $\Omega^{-1} \text{ m}^{-1}$)	15.8×10^6
Electrical conductivity of liquid (σ_L , $\Omega^{-1} \text{ m}^{-1}$)	8.8×10^{-6}
Temperature gradient (G , K m^{-1})	60×10^2
Kinematic viscosity (ν , m s^{-1})	1.2×10^{-7}
Density (ρ , kg m^{-3})	7.14×10^3

Acknowledgments

This work is supported by the National 973 Project (Nos. 2014CB643403 and 2011CB610404), the European Space Agency through the IMPRESS project, Natural Science Foundation of China

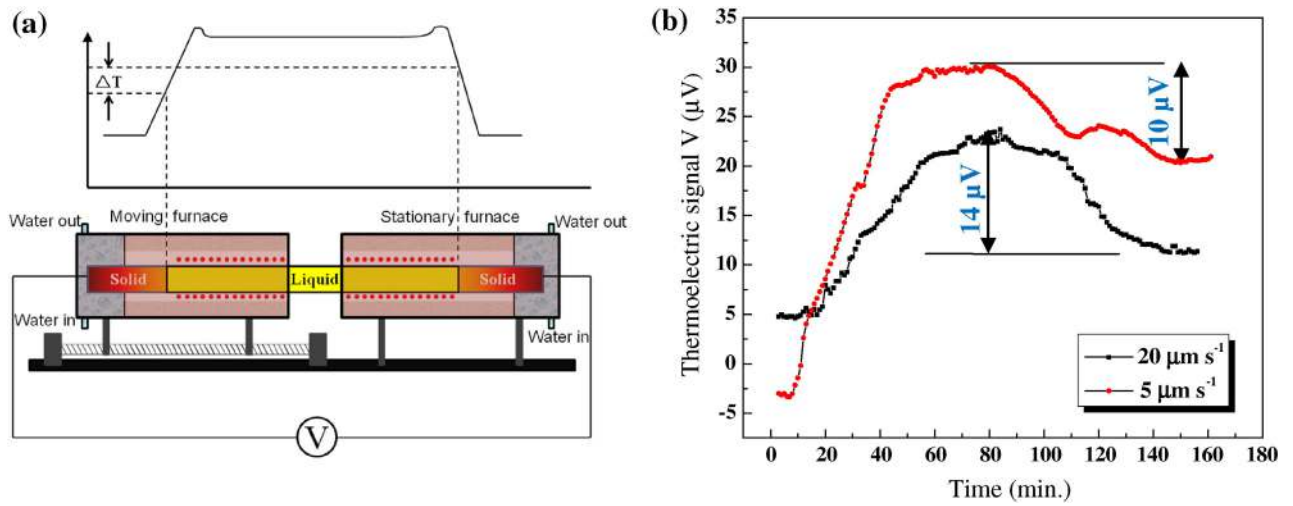


Fig. 11. (a) Schematic diagram of the MEPHISTO apparatus and (b) Seebeck response obtained for Zn-5 wt.% Cu alloy at various growth speed.

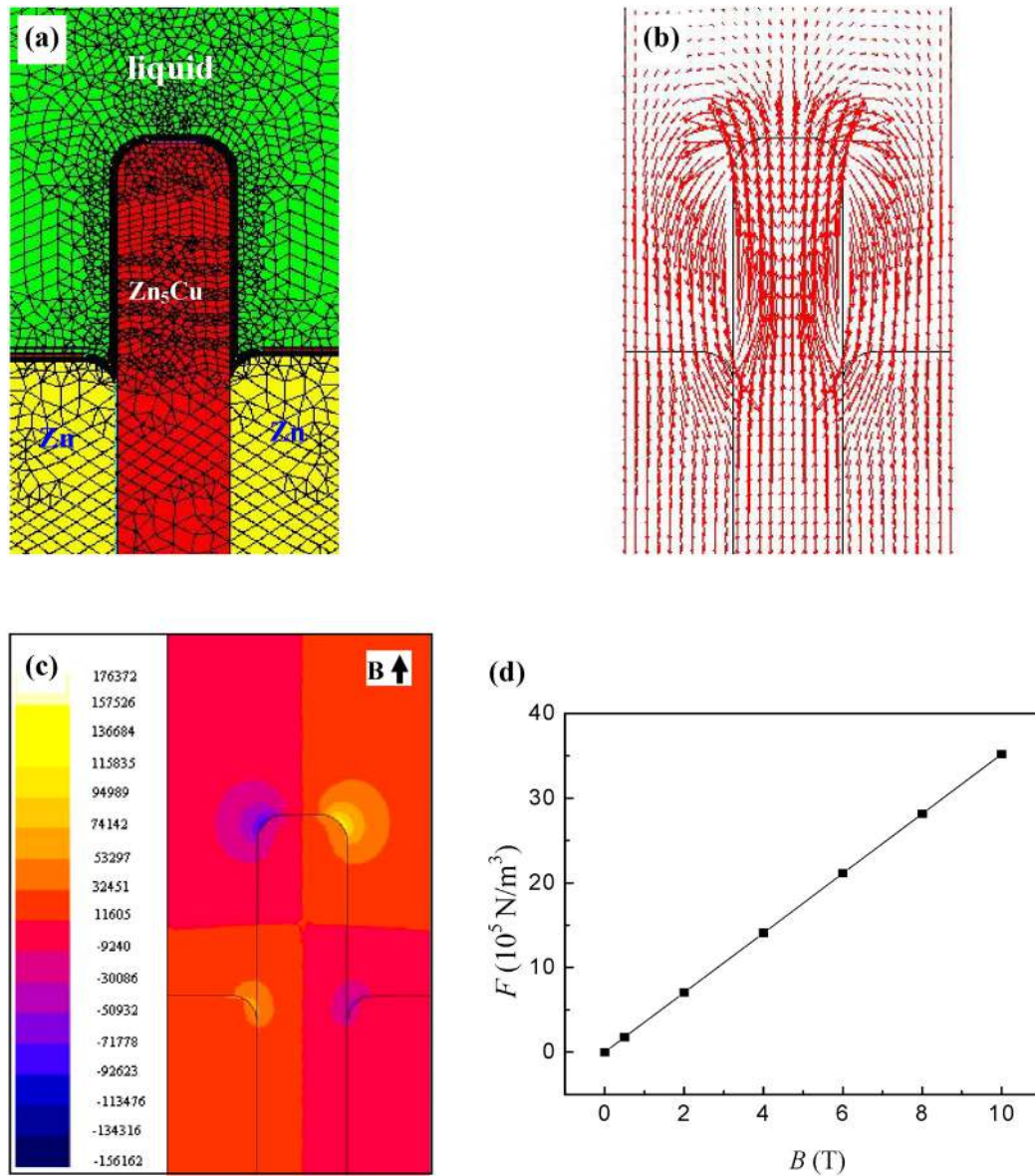


Fig. 12. Computed thermoelectric magnetic effects around the modeled liquid/solid interface during directional solidification of the Zn-Cu alloys under a 0.5 T magnetic field: (a) Mesh for the numerical simulation; (b) thermoelectric current streamlines near the interface (in A/m); (c) thermoelectric magnetic force in liquid and solid near the liquid/solid interface (in N/m^3); and (d) value of the thermoelectric magnetic force acting on the solid as a function of the magnetic field intensity.

(Nos. 51271109, 51171106 and 51225401) and the Science and Technology Committee of Shanghai (No. 14JC1491400).

References

- [1] T.B. Massalski, Binary Alloy Phase Diagrams, American Society for Metals, Metals Park, OH, 1986.
- [2] D.R. Uhlmann, G.A. Chadwick, *Acta Metall.* 9 (1961) 835.
- [3] W.J. Boettinger, *Metall. Trans.* 5 (1974) 2023.
- [4] F. Fredriksson, T. Nylen, *Metals Sci.* 16 (1982) 283.
- [5] J.H. Lee, J.D. Verhoeven, *J. Cryst. Growth* 144 (1994) 353.
- [6] T. Izumi, Y. Shiohara, *J. Mater. Res.* 7 (1993) 16.
- [7] T. Izumi, Y. Nakamura, Y. Shiohara, *J. Cryst. Growth* 128 (1993) 757.
- [8] R. Glardon, W. Kurz, *J. Cryst. Growth* 51 (1981) 283.
- [9] K.G. Knoch, B. Reinsch, G. Petzow, *Z. Met.* 85 (1994) 350.
- [10] S. Asai, *Sci. Technol. Adv. Mater.* 1 (2000) 191.
- [11] X. Li, A. Gagnoud, Y. Fautrelle, Z.M. Ren, R. Moreau, C. Esling, *Acta Mater.* 60 (8) (2012) 3221.
- [12] OIM. User's Manual. EDAX-TSL E. Mahway; 2005.
- [14] X. Li, Y. Fautrelle, Z.M. Ren, *J. Cryst. Growth* 306 (2007) 187.
- [15] J.A. Shercliff, *J. Fluid Mech.* 91 (1979) 235.
- [16] P. Lehmann, R. Moreau, D. Camel, R. Bolcato, *Acta Mater.* 46 (1998) 4067.
- [17] D.J. Ma, L. Hou, X. Li, Y. Fautrelle, Z.M. Ren, K. Deng, B. Saadi, F. Debray, *Mater. Lett.* 106 (2013) 313.
- [18] J.D. Hunt, *Mater. Sci. Eng.* 65 (1984) 75.
- [19] A. Rouzaud, J. Comera, P. Contamin, B. Angelier, F. Herbillon, J.J. Favier, *J. Cryst. Growth* 129 (1993) 173.
- [20] J.J. Favier, J.P. Garandet, A. Rouzaud, D. Camel, *J. Cryst. Growth* 140 (1994) 237.
- [21] R.P. Huebener, Thermoelectricity in metals and alloys, in: F. Seitz, D. Turnbull (Eds.), *Solid State Physics*, vol. 27, Academic Press, New York 1972, p. 64.
- [22] A. Makradi, J.G. Gasser, S. Belouettar, *J. Non-Cryst. Solids* 356 (2010) 400.
- [23] N.F. Mott, *Proc. R. Soc. Lond. A* 146 (1934) 465.